Diiodo-BODIPY sensitizing of $[Mo_3S_{13}]^{2-}$ cluster for noble metal-free visible light-driven hydrogen evolution within a polyampholytic matrix

Daniel Costabel,[a‡]* Afshin Nabiyan,[a‡] Avinash Chettri,[bc] Franz Jacobi,[a] Magdalena Heiland,[d] Julien Guthmuller,[e] Stephan Kupfer,[b] Maria Wächtler,[bc] Benjamin Dietzek-Ivanšic,[bcf] Carsten Streb,[d] Felix H. Schacher[af] and Kalina Peneva[af]*

[a]Institute of Organic Chemistry and Macromolecular Chemistry, Friedrich Schiller University Jena, Lessingstraße 8, 07743 Jena, Germany.

[b]Institute of Physical Chemistry, Friedrich Schiller University Jena, Helmholtzweg 4, 07743 Jena, Germany.

[c]Leibniz Institute of Photonic Technology Jena, Albert-Einstein-Straße 9, 07745 Jena, Germany.

[d]Institute of Inorganic Chemistry I, Ulm University, Albert-Einstein-Allee 11, 89081 Ulm, Germany.

[e]Institute of Physics and Computer Science, Faculty of Applied Physics and Mathematics, Gdansk University of Technology, 80233 Gdansk, Poland.

1

[f]Center for Energy and Environmental Chemistry and Jena Center of Soft Matter, Friedrich Schiller University Jena, Philosophenweg 7a, 07743 Jena, Germany.

Keywords

BODIPY, Hydrogen Evolution, Quantum Chemistry, Photocatalysis, Thiomolybdate

Abstract

We report on a photocatalytic setup, that utilizes the organic photosensitizer (PS) diiodo-BODIDPY and the non-nprecious metal-based hydrogen evolution reaction (HER) catalyst $(NH_4)_2[Mo_3S_{13}]$ together with a polyampholytic unimolecular matrix poly(dehydroalanine)-*graft*-poly(ethylene glycol) (PDha-*g*-PEG) copolymer in aqueous media. The system shows exceptionally high performance with turnover numbers ($TON > 7300$) and turnover frequencies ($TOF > 450$ h^{-1}) which are typical for noble-metal-containing systems. Excited-state absorption spectra reveal the formation of long-lived triplet state of the PS in both aqueous and organic media. The system is a blueprint for developing noble-metal free HER in water. Component optimization, *e.g.* by modification of the *meso* substituent of the PS and the composition of the HER catalyst is further possible.

Introduction

Artificial photosynthesis is one major approach that can overcome fossil fuel dependency especially in form of light-driven hydrogen evolution for solar fuel production.[1, 2] However, most systems utilize precious metal-based complexes as both, their light sensitive materials as well as their catalytically active sites, limiting their application to model systems for mechanistic investigations.[3-7] The development of catalysts composed of non-noble metals has led to a variety of different materials and molecular proton reduction systems such as graphitic carbon nitride[8, 9], iron-iron hydrogenase mimics[10-13], and thiomolybdate clusters.[14, 15] On the other hand, development and application of photosensitizers (PSs) based on earth-abundant elements have been limited to a few example due to their mostly hydrophobic nature and fast charge recombination.[16-19] One strategy to overcome these deficits relies on the involvement of macromolecular templating agents as soft matter matrices. Stupp and coworkers reported light-driven hydrogen evolution by thiomolybdate clusters sensitized by perylene monoimides (PMI) in hydrogels based on PDDA.[20] Recently, we reported two different polyampholytic graft copolymers poly(dehydroalanine)-graft-poly(ethylene glycol) (PDha-g-PEG) and poly(dehydroalanine)-graft-(n-propyl phosphonic acid acrylamide) (PDha-g-PAA) assisting organic PSs based on PMI and Eosyn Y in photocatalytic hydrogen evolution with $(NH_4)_2[Mo_3S_{13}]$.[21-23] However, the application of those dyes suffers from fast charge recombination and hardly accessible triplet states. Amongst organic dyes, 4,4-difluoro-4-bora-3a,4a-diaza-s-indacene (BODIPY) based chromophores have shown high potential in photocatalytic applications due to their readily accessible triplet excited states, showing long lifetimes due to reduced recombination rates and, thus, enlarging the timeframe for electron-transfer.[24-26] Initially applied in biomedical imaging[27-29] where BODIPYs served as fluorescent

3

tags for lipids and peptides, the application scope of BODIPY-based dyes has broadened. Amongst others, You and coworkers utilized iodo substituents to enable intersystem crossing (ISC) to the
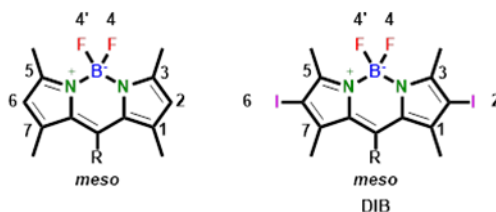

Figure 1. General structure and positions of 1,3,5,7-tetramethyl BODIPY and 2,6-diiodo-1,3,5,7-tetramethyl BODIPY (DIB).

triplet excited state for photodynamic therapy.[30, 31] Zhao and coworkers made use of the easily accessible triplet state for triplet-triplet annihilation[32, 33], reaching triplet state lifetimes up to 66.3 µs. Additionally, BODIPY based dyes have been applied in dye-sensitized solar cells (DSSC)[34-37] with a donor-BODIPY-acceptor architecture as well as in artificial photosynthetic systems towards photocatalytic hydrogen evolution.[38-40]

Lately, investigations regarding the scope of applications on BODIPYs for photocatalysis have been carried out with cobaloximes as hydrogen evolution reaction (HER) catalyst. Typically, 1,3,5,7-tetramethyl BODIPY bearing iodo-substituents in 2- and 6-position (**DIB**, Fig. 1) utilized pyridine or aniline in the *meso* position for electrostatic interaction towards the cobaloxime catalyst.[41, 42] These investigations point out the high demand on noble metal-free, organic PSs in photocatalytic applications. Sommer and coworkers reported a BODIPY bearing a *para*-(3-methyl)pyridyl substituent in *meso* position which achieved a maximum turnover number (*TON*) of 31.[43] With their *ortho*-pyridyl substituent in *meso* position, Zhao and coworkers were capable of sensitizing cobaloximes in aqueous solutions with triethanolamine (TEOA) as a sacrificial donor, reaching *TON*s up to 85 under a reductive quenching mechanism, which proves catalytic

4

activity but does not compete with sensitization by noble metal complexes such as $[Ru(bpy)_3]^{2+}$ and $[Ir(ppy)_2bpy]^+$ in terms of *TON*.[44, 45] On the other hand, many successful reported photocatalytic systems with BODIPY PSs rely on noble metal molecular HER catalysts based on either palladium or platinum central atoms.[46] Beweries and coworkers synthesized a DIB with a mesityl substituent in *meso* position sensitizing a binuclear $Pd_2(PPh_3)_2Cl_4$ catalyst in the presence of triethylamine (TEA) in THF/water mixtures for *TON* up to 305.[47, 48] Combining 2,6-diethyl-1,3,5,7-tetramethyl BODIPY with a phenyldithiolato-bipyridyl platinum(II) complex *via meso* position was reported by Eisenberg and coworkers reaching a *TON* of up to 40.000 with platinated TiO_2 upon sequential addition of ascorbic acid as their sacrificial electron donor over 12 days (turnover frequency (*TOF*) 139 h^{-1}).[49, 50] Lately, polyoxometalates have been reported for covalent conjugation to BODIPY PSs to create organic-inorganic hybrid materials towards unimolecular photocatalysts.[51, 52]

This work aims at developing photocatalytic hydrogen evolution systems that circumvent noble metal nuclei in both the visible light-active and the catalytically active component. In our previous work, the thiomolybdate cluster $[Mo_3S_{13}]^{2-}$ was identified as an ideal candidate that provided high photocatalytic activity with $[Ru(bpy)_3]^{2+}$ PSs.[14, 53, 54] Furthermore, the molecular catalyst evolved molecular hydrogen with organic, hydrophobic dyes in aqueous solution by the addition of a unimolecular soft matter matrix, a polyampholytic graft copolymer PDha-*g*-PEG.[22] The applied graft copolymer does not only act as a solubilizing agent but also shows that supramolecular architecture in photocatalysis can boost activity and stability of the investigated combination of photoactive and catalytic component. Herein, we report on a photocatalytic system, that combines noble metal-free BODIPY PSs and a molecular catalyst $[Mo_3S_{13}]^{2-}$ of earth-abundant composition in aqueous solution. This system is not only suitable as a noble metal-free model but does actually

5

compete with benchmark PSs ($[Ru(bpy)_3]^{2+}$, $[Ir(ppy)_nbpy]^+$) and catalysts (cobaloximes, $[Pt(bpy)Cl_2]$, platinated TiO_2) in terms of photocatalytic activity and can serve as a platform for the testing and preparation of sustainable and efficient PS/CAT pairs that are integrable via further modification via the *meso* substituent.

Experimental Section

Materials: All solvents and chemicals were purchased in commercial grade (Acros, Alfa Aeser, Deutero, Eurisotop, Fisher, Grüssing, Merck, Roth, Sigma Aldrich, TCI and VWR) and unless otherwise stated, used as obtained. The progress of all reactions was monitored by thin-layer chromatography (Merck 60 F254). Column chromatography was performed with Macherey-Nagel silica gel 60 (grain size 0.04-0.063 nm).

NMR Spectroscopy: NMR spectra were recorded on a Bruker Avance 300. Spectra were referenced to residual solvent signals ($CDCl_3$), chemical shifts are reported in parts per million.

UV-Vis Absorption: UV/Vis spectra were recorded on an Agilent Technologies Cary 60 UV-Vis at room temperature. Solutions were prepared to a concentration between 1 and 10 μM in dichloromethane.

Fluorescence Emission: Fluorescence emission was recorded on a Jasco FP 8300 in DCM at room temperature. The absorption of each solution was adjusted to 0.05 in the respective maximum.

DLS: DLS measurements were performed using an ALV laser CGS3 Goniometer equipped with a 633 nm HeNe laser (ALV GmbH, Langen, Germany) at 25°C and at a detection angle of 90°. The CONTIN analysis of the obtained correlation functions was performed using the ALV 7002 FAST Correlator Software.

6

TEM: TEM images were acquired with 200 kV FEI Tecnai G2 20 equipped with 4k × 4k Eagle HS CCD and a 1k × 1k Olympus MegaView camera for overview images.

Cyclic voltammetry: Cyclic voltammetry was carried out in a setup of three electrodes with a Gamry Instruments Reference 600 Potentiostat. A carbon electrode was used as the working electrode, Ag/Ag+ in acetonitrile as a reference electrode and platinum as the counter electrode. The three electrode setup was placed in a sealed flask with 6 ml of 0.1 M tetrabutylammonium hydroxide solution in DCM and 2 to 5 μmol of the investigated compound. 1 ml of DCM was added before the solution was degassed with a nitrogen stream until the total volume decreased to 6 ml. Measurements were referenced against the Fc^+/Fc couple.

Detailed description on the synthesis, photocatalytic hydrogen evolution, steady state and nanosecond transient absorption spectroscopy, quantum chemistry and NMR spectra can be found in the supporting information file.

Results and Discussion

Synthesis and Characterization

For the synthesis of *meso*-substituted 2,6-diiodo-1,3,5,7-tetramethyl-BODIPYs (**DIB**), condensation of 2,4-dimethyl-1*H*-pyrrole with the respective aldehydes in DCM or THF with catalytic amounts of trifluoroacetic acid were applied[55-59] with the exception of **DIB-H** bearing only a hydrogen atom in the *meso* position, which utilized trimethyl orthoformate and one equivalent of *p*-toluenesulfonic acid (Scheme 1).[60] The variation in the *meso* substituent gives a library of **DIBs** with varying properties and allows for subsequent modification, *e.g.* via cross-coupling reactions (**DIB-PhBr**) or anchoring (**DIB-PhOH**). For the subsequent oxidation, typical procedures involve either DDQ or the better soluble but less active *p*-chloranil. The intermediate

7

was isolated for the unsubstituted starting benzaldehyde, however, on all other occasions, the formation of BODIPY was carried out as a one- pot-reaction, since the purification of tetramethyl-
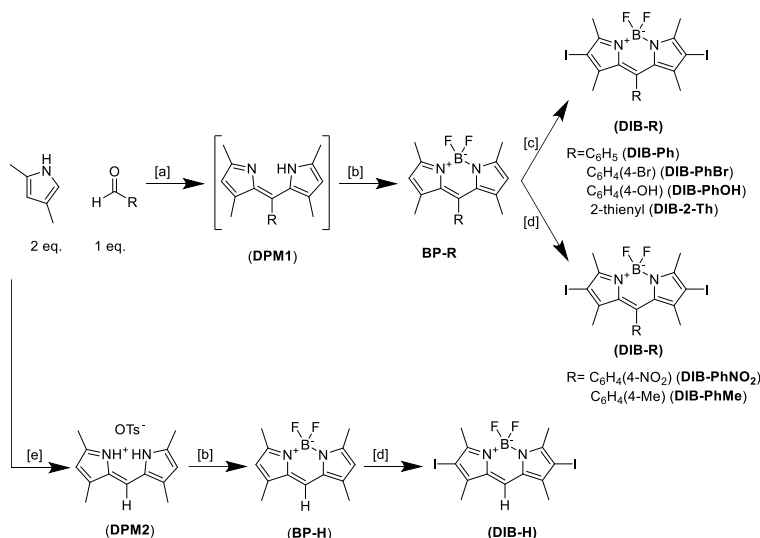
Scheme 1. Synthetic route for the different 2,6-diiodo-1,3,5,7-tetramethyl-BODIPYs (DIB). [a] 1. TFA, DCM (or THF), r.t. 3-14 h; 2. DDQ (or *p*-chloranil). [b] 1. TEA (or DIPEA), DCM, r.t.; 2. BF_3-OEt_2, 0°C-r.t., 2-14 h. [c] I_2/ HIO_3, EtOH/ DCM, -20°C-60°C, 20 min - 2h. [d] NIS, DCM (or THF), r.t. to 45°C, 3-14 h. [e] Trimethyl orthoformate, *p*-TsOH, toluene, r.t., 2h.

phenyl-dipyrromethene goes along with severe product loss. TEA or DIPEA were used as a base with subsequent addition of the same volume of boron trifluoride etherate.[61] Depending on the BOPIPY, two different iodination procedures were utilized, one involving iodine and iodic acid in mixtures of ethanol and DCM (**DIB-Ph/PhBr/PhOH/2-Th**).[62, 63] The other option uses *N*-iodosuccinimide (NIS) as an iodinating agent in DCM (**DIB-PhNO2/PhMe/H**).[59, 61, 63, 64] While the latter iodinating procedure is much more straightforward, electron rich *meso* substituents get iodinated by NIS in favour of the BODIPY structure. ^{1}H-NMR spectra were in agreement with the literature; however, the yields were only between 50% and 90% of the reported ones. The formation of the chromophore requires four steps and it can be carried out in one pot with

8

reasonable yields from small molecular building blocks of simple architecture without isolating and purifying the intermediates.

Absorption, Emission Spectroscopy and Cyclic Voltammetry

The photophysical properties of the chromophores were investigated in DCM. All spectra showed absorption maxima between 533 and 548 nm with extinction coefficients between 44.200 (**DIB-PhNO₂**) and 85.000 M^{-1}cm^{-1} (**DIB-Ph**). The influence of the *meso* substituent on the photophysical properties was found to be relatively small with the most hypsochromically shifted absorption maximum for **DIB-PhMe** (533 nm) and the most bathochromically shifted compound **DIB-2-Th** (548 nm) (Fig. 2). It is noteworthy that both electron withdrawing groups(**DIB-NO₂**) and electron donating groups (**DIB-2-Th**) caused bathochromic shifts compared to phenyl substituted **DIB-Ph**. Similar shifts can be accounted for the emission maxima between 547 and 561 nm (Fig. 2), the respective stokes shifts ranged between 336 and 562 cm^{-1}.
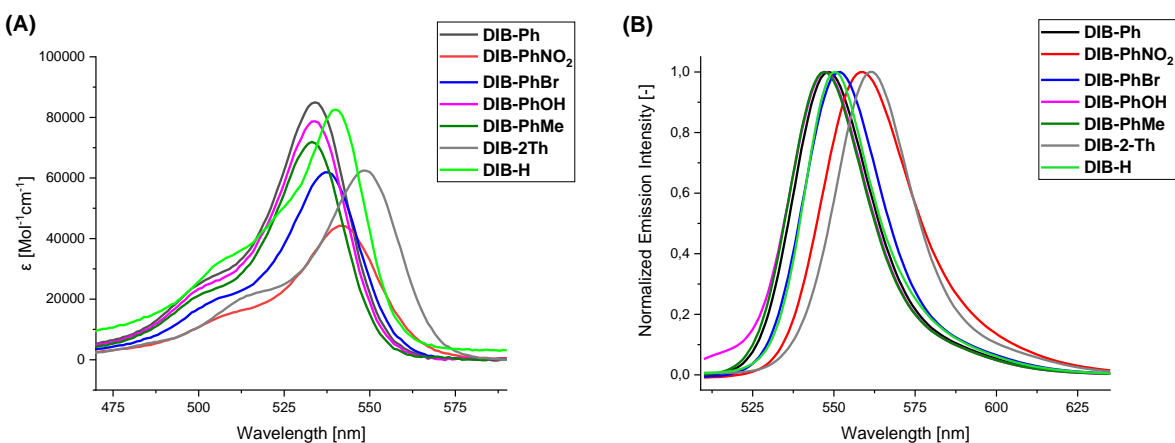

Figure 2. (A) Absorption spectra of DIBs in DCM (5-10 •10^{-7} mol/L); (B) Normalized Fluorescence emission spectra of DIBs in DCM.

Cyclic voltammetry (CV) was carried out to examine the redox properties of the PSs, i.e., to determine suitable hydrogen evolution catalysts and sacrificial electron donors. The reduction potentials of the dyes were spread between -1.30 and -1.47 V (vs Fc/Fc$^+$, Fig. S2) and were 0.10
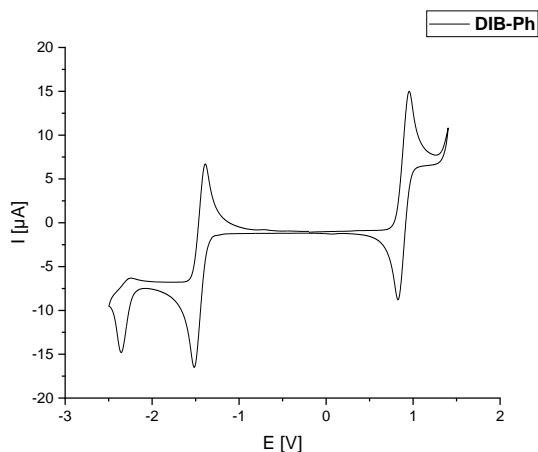

Figure 3. Cyclic voltammogram of DIB-Ph in DCM, 0.1 M Bu$_4$NPF$_6$, 20°C, 50 mV•s^{-1} referenced to the Fc/Fc$^+$ couple.

and 0.27 V above the reduction potential of $[Mo_3S_{13}]^{2-}$ (depicted in Fig. 3 for **DIB-Ph** and Table 1) which can be considered a suitable driving force for the desired (light-induced) electron transfer. As expected, the strong electron withdrawing effect of the nitro group of **DIB-PhNO₂** is manifested in the lowest reduction potential, however, the influence of electron donating groups to the chromophore is rather small, *e.g.* comparing **DIB-Ph** (-1.45 V) to **DIB-PhOH** and **DIB-PhMe** (both -1.47 V). **DIB-H** is the only **DIB** derivative for which an irreversible electrochemical reduction event (-1.42 V onset vs. Fc/Fc$^+$) was observed. Additionally, it is the only chromophore showing an additional irreversible oxidation feature in the backsweep of the reduction side. We

10

Table 1. Spectroscopic, electrochemical, and calculated properties of DIBs. [a] DCM, 20°C. [b] DCM, 0.1 M Bu₄NPF₆, 20°C, 0.05 V•s⁻¹, vs. Fc/Fc⁺ (*onset potential due to irreversibility; **Onset potential in DMF; ***in aqueous solution vs. SCE, calculated to Fc/Fc⁺ by subtraction of 0.38 V).

DIB	λ_{max} [nm][a]	λ_{Em} [nm][a]	E_{ox1} [V][b]	E_{red1} [V][b]
-Ph	534	548	0.89	-1.45
-PhNO₂	542	559	0.95	-1.30
-PhBr	537	552	0.91	-1.41
-PhOH	534	547	0.83	-1.47
-PhMe	533	547	0.87	-1.47
-2-Th	548	561	0.91	-1.34
-H	540	550	0.86	-1.42*
			-0.44*	
[Mo₃S₁₃]²⁻	-	-	-	-1.20**
AA⁶⁵***	-	-	0.08	

assume that both deviating phenomena are caused by the structural difference in the *meso* position compared to the other **DIBs**. The oxidation potentials of most derivatives were located between 0.83 V (**DIB-PhOH**) and 0.95 V (**DIB-PhNO₂**). In contrast to the reduction potential, both electron donating groups (**DIB-PHOH**: 0.83 V) and withdrawing groups (**DIB-PhNO₂**: 0.95 V) show a moderate influence on the oxidation potential (**DIB-Ph**: 0.89 V). Beyond the fine tuning of the PS reduction potential, investigating several derivatives gives platforms for further chemical modifications like anchoring the PS via the *meso* substituent.

Photocatalytic Hydrogen Evolution

Hierarchical structuring of photocatalytic components within, *e.g.* a soft matter matrix can be beneficial for the catalytic activity, if compared to homogeneous systems.[20, 22, 23] Polymeric templates are capable of solubilizing hydrophobic dyes in aqueous media. Furthermore, they can bring components with different properties such as charged metal cluster catalysts, hydrophobic photoactive materials and sacrificial electron donors in close spatial proximity, while also
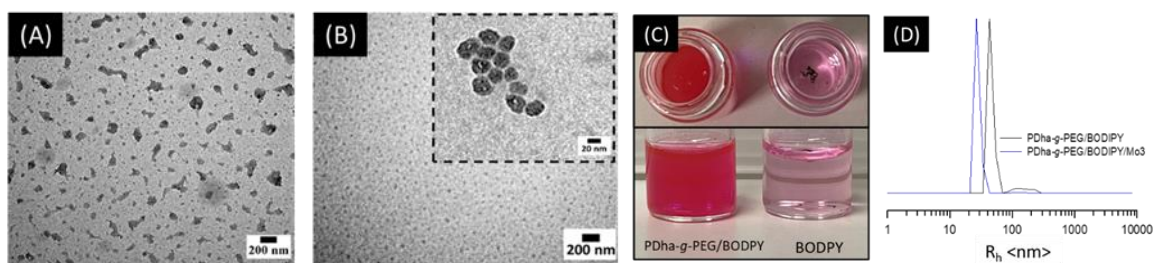

Figure 4. (A) TEM micrographs of DIB-Ph with PDha-g-PEG. (B) TEM micrograph of DIB-Ph and [Mo3S13]$^{2-}$ with PDha-g-PEG. (C) DIB-Ph with (left) and without (right) PDha-g-PEG in water. (D) DLS CONTIN plot for DIB-Ph with PDha-g-PEG and DIB-Ph with PDha-g-PEG and [Mo3S13]$^{2-}$.

protecting the substances from photodegradation. In our case, the otherwise water insoluble BODIPY photosensitizers were readily dispersed in water using the polyampholytic graft copolymer poly(dehydroalanine)-*graft*-poly(ethylene glycol) – thereby forming nanometer-sized nanoreactors in aqueous solution (Fig. 5). The synthesis of the graft copolymer was carried out in three steps. First, radical polymerization of tert-Butoxy carbonyl aminomethyl acrylate (*t*BAMA) to P*t*BAMA was carried out, followed by acidic deprotection to remove the Boc group and in the last step, corresponding deprotected polymers was modified with the epoxy end functionalized PEG (1000 g/mol) (Fig. S1). Kinetic studies on the last synthetic step revealed that a maximum

degree of functionalization (DoF, defined as the amount of functionalized repeat units in %) of ~15% can be reached after 24 h, when 0.2 equivalent of PEG1000 was used. The obtained dispersion was subjected to dynamic light scattering (DLS, Fig. 4D) and transmission electron microscopy (TEM, Fig. 4A) to investigate the size and morphology of the formed nanoobjects, revealing mostly spherical morphology and size distribution between 43-140 nm in radii. However, as we demonstrated in our previous reports, $[Mo_3S_{13}]^{2-}$ can also be solubilized using PDha-based graft copolymers.[22, 23] The obtained dispersion was investigated towards its
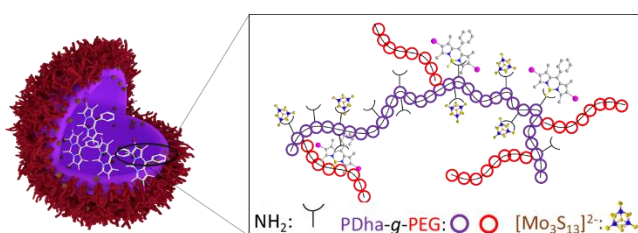

Figure 5. Schematic illustration of the CAT-PS-polymer interactions and formation of nanoaggregates.

morphology and particle size. An average size of 26 nm in radius and a well-defined size distribution are an indication of the electrostatic interaction between PDha-*g*-PEG featuring also positive charges (-NH$_3^+$,pH<5) and negatively charged $[Mo_3S_{13}]^{2-}$. After the formation of well-defined nanospheres, systems containing **DIB-Ph**/$[Mo_3S_{13}]^{2-}$/PDha-*g*-PEG were tested for light-driven hydrogen evolution experiments in the presence of ascorbic acid as sacrificial electron donor (detailed description in the Supporting Information). Earlier studies showed that photosensitization of the $[Mo_3S_{13}]^{2-}$ catalyst is required to drive hydrogen evolution, while irradiation of the catalytic complex alone does not lead to light-driven HER.[54, 66] Initially, the

13

optimal concentration of the graft copolymer matrix was investigated. Solutions containing 2 mg/ml of PDha-*g*-PEG outperformed five- to sixfold compared to solutions with 1.5, 2.5 and 3 mg/ml with a *TON* of 1190 (Fig. 6A). This result indicates the critical role of the graft copolymer in the formation of the nanoobjects. Lowering the polymer/**DIB** ratio results in less stable aggregates with high content of hydrophobic **DIB-Ph**, which suffer from precipitation over time. On the other hand, higher concentration of graft copolymer reduces the activity, we hypothesize this to happen by blocking of the light-harvesting **DIB-Ph** via scattering of the polymer dispersion or, as an alternative, by simply diluting the amount of photo-active component. Subsequent optimization of the photosensitizer concentration showed that a saturation limit is reached at a concentration of 75 µM and a total *TON* of 1827 (Fig. S3). The concentration of ascorbic acid in
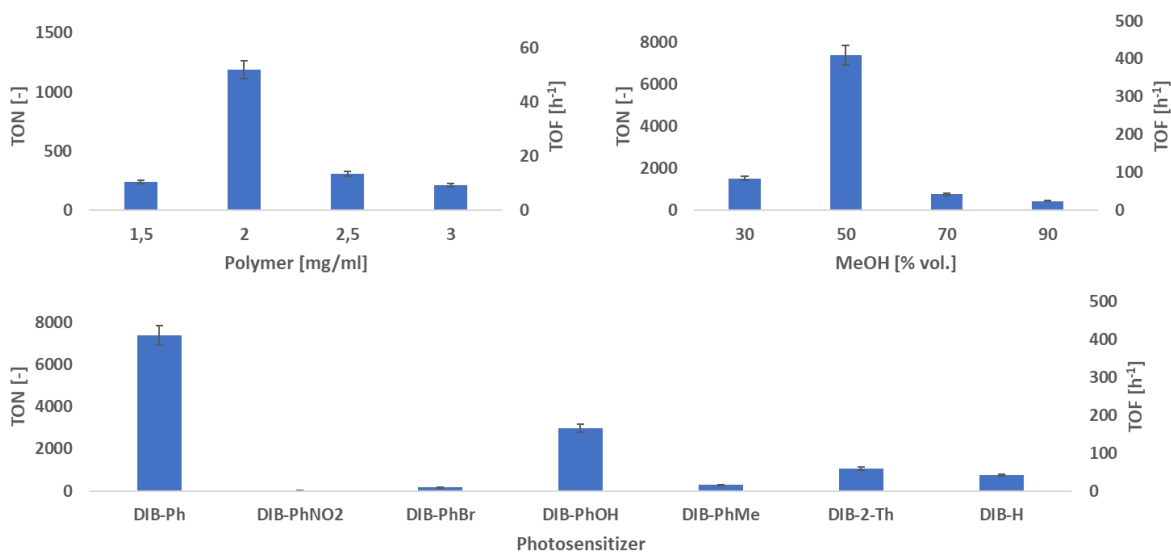

Figure 6. Photocatalytic hydrogen evolution with $(NH_4)_2[Mo_3S_{13}]$, DIB-Ph, ascorbic acid, PDha-*g*-PEG in water over 20 h irradiation (λ=530 nm). (A) Optimization of PDha-*g*-PEG concentration (mg/ml). (B) Optimization of methanol water ratio. (C) Comparison of DIBs under optimized conditions. TON and TOF values are calculated with respect to the catalyst.
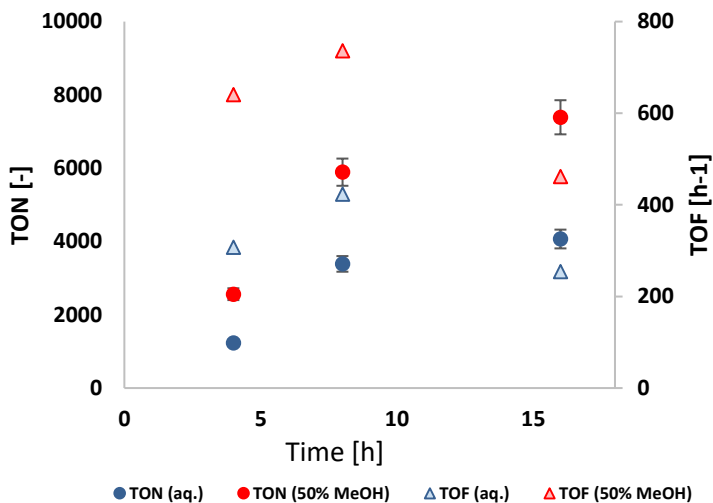
Figure 7. Time-dependent hydrogen evolution with DIB-Ph under optimized conditions with 50% methanol (red) and without methanol (blue). TON and TOF values are calculated with respect to the catalyst.

the photocatalytic solutions showed only a minor influence (*TON* between 2123 to 2277), however, above this concentration, precipitation of the dye was observed as well (Fig. S3). A remarkable impact on the photocatalytic performance was observed by addition of methanol. In contrast to a previous report on $[Mo_3S_{13}]^{2-}$-based photocatalytic systems where the ideal solvent mixture was described as MeOH:H$_2$O, 10:1, v:v,[53] we observed the highest performance at 50 vol-% MeOH, giving a *TON* of 7389, while mixtures containing 30 vol-%, 70 vol-% and 90 vol-% MeOH gave *TONs* of 1528, 768, and 452, respectively (Fig. 6B). Photocatalytic activity for the different **DIBs** ranged from *TONs* 45 to 7389 (Fig. 6C). While **DIB-Ph** (*TON* = 7389) noticeably shows the highest activity,

15

Table 2. Photocatalytic HER performance of MoS catalysts with different photosensitizers and BODIPY photosensitizers with different catalysts.

	CATALYST	PHOTOSENSITIZER	TON [-]	TOF $[H^{-1}]$	REFERENCE
1	$[Mo_3S_{13}]^{2-}$	$[Ru(bpy)_3]^{2+}$	41.000	1708	[54]
2	$[Mo_3S_{13}]^{2-}$	$[Ru(bpy)_3]^{2+}$	ca. 510	102	[66]
3	$[Mo_3S_{13}]^{2-}$	$[Ru(bpy)_3]^{2+}$	1.630	272	[53]
4	$[Mo_3S_{13}]^{2-}$	9-Me-PMI-N-$(CH_2)_5CO_2Na$	478	27	[67]
5	$[Mo_3S_{13}]^{2-}$	9-nPr-PMI-N-$(CH2)_5CO_2Na$	11.000	110	[68]
6	$[Mo_3S_{13}]^{2-}$	1,7,9,10-SePh$_4$-PMI-N-$(CH_2)_5CO_2Na$	104	1.6	[22]
7	$\mathbf{[Mo_3S_{13}]^{2-}}$	**DIB-Ph**	**7389**	**462**	**This work**
8	Co(dmg)$_2$Cl	DIB-3-Py	85	17	[44]
9	Pd$_2$Cl$_4$(PPh$_3$)$_2$	DIB-Mes	305	15	[47]
10	TiO$_2$/Pt	BODIPY-Pt-complex	40.000	139	[50]

DIB-PhOH (2997) is in the same order of magnitude. **DIB-2-Th** (*TON* = 1067) and **DIB-H** (*TON* = 754) display about one order of magnitude less photocatalytic performance. Except for **DIB-PhNO₂** (*TON* = 45)there is no explicit trend between either spectroscopic or electrochemical properties and the photocatalytic performance. However, TDDFT simulations revealed the presence of low-lying and accessible CT state in **DIB-PhNO₂** as well as in **DIB-Ph-Br** – in contrast to **DIB-Ph**. Therefore, the performed quantum chemical simulations point to an additional excited-state relaxation channel potentially hampering catalytic activity. **DIB-Ph** displays a *TOF*

of 641 h^{-1} over the first 4 h of irradiation. The *TOF* increases over 8 h to 736 h^{-1}. Over 16 h, the turnover frequency of our noble metal-free photosynthetic platform reaches 462 h^{-1} under optimized conditions (Fig. 7). The photocatalytic performance of this setup regarding both *TON* and *TOF* is exceptionally high for an organic PS combined with a noble metal-free HER catalyst and is well within the photocatalytic performance of both noble metal-based PSs and catalysts (Table 2). We further elucidated the crucial role of the templating agent in this setup, by testing a variety of other polymer structures, amongst them linear PEG and various amphiphilic poly-methacrylamide terpolymers, however, none exceeded 7% of the activity reached by employing PDha-*g*-PEG as polyampholytic matrix (Fig. S3). The activity of the [Mo$_3$S$_{13}$]$^{2-}$ HER catalyst could be boosted by the presence of ammonium ions,[69] therefore we hypothesized that the significantly higher performance of PDha-*g*-PEG compared to all other tested polymers is partially due to the presence of protonated amines in the side chain of PDha-*g*-PEG.

Quantum Chemistry

The energies and geometries of the lowest singlet (S1) and triplet (T1-T3) excited states of DIB-Ph were investigated with time-dependent density functional theory (TDDFT) calculations (Fig. 8). The effects of the solvent DCM are described by the polarizable continuum model. The calculations reveal that after excitation in the bright S1 state (f=0.595, Table S1), intersystem crossing occurs most efficiently toward the π→π* triplet states T2 and T3. This is justified by the values of the spin-orbit couplings (of up to 15 and 9 cm-1, Fig. S6) and by the energetic proximity of the S1, T2 and T3 states at all considered geometries. Spin-orbit couplings have been obtained along a linear-interpolated internal coordinate connecting the fully optimized equilibrium structures of the (singlet) ground state and the optical accessible S1 state. Geometrical relaxation
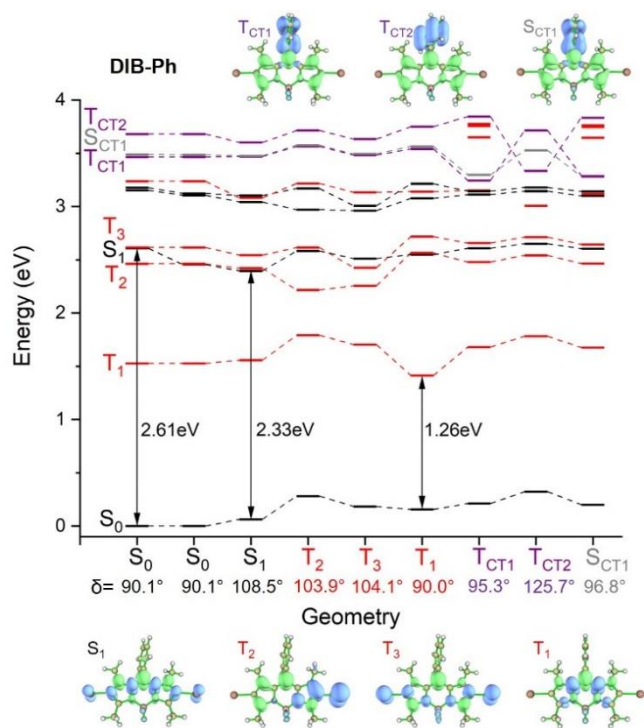
17

Figure 8. Calculated (B3LYP/def2-SVP) energy levels diagram for DIB-Ph in DCM, nonequilibrium solvation at S0 geometry (left), equilibrium solvation at other geometries. Charge density difference (CDD) of the states at their optimized geometry, blue (hole) and green (electron). DIB-Phenyl dihedral angle (δ).

of these states also leads to a rotation of the phenyl ring, which adopts non-orthogonal positions ($\delta \approx 104$-$109°$) with respect to the DIB fragment. After population of the T2 and T3 states, the system is expected to relax to the lowest triplet state T1, by internal conversion in which the phenyl ring has an orthogonal orientation. Similar calculations performed on DIB-PhBr and DIB-PhMe (Figs. S4, S5) show that substitution of the phenyl by Br or Me has a little impact on the energies and geometries of the S1, T1, T2 and T3 states as well as on the SOCs of the S1 state with these triplet states (Fig. S6). For example, going from DIB-Ph to DIB-PhBr small energy shifts of -

18

0.013 eV and -0.024 eV are obtained for the vertical absorption and emission energies, respectively. These values are in good agreement with the experimental shifts of -0.013 eV and -0.016 eV deduced from the maxima of absorption and emission (Fig. 2). The small effect of substitution on the S1 and T1-T3 states is due to the fact that these states involve $\pi \rightarrow \pi^*$ transitions localized only on the DIB chromophore (see CDDs on Fig. 8) and are therefore little affected by changes occurring on the phenyl ring. This indicates that the observed differences in photocatalytic activity in these systems (Fig. 6) are not related to changes of properties in the initially populated singlet and triplet states.

Excited states involving a charge transfer (CT) between the phenyl ring and the **DIB** centre are expected to be more sensitive to substitution. In the case of **DIB-Ph**, the lowest CT states (S_{CT1}, T_{CT1} and T_{CT2}) feature a CT from the phenyl group toward the **DIB** core (see CDDs on Fig. 8). However, these states remain significantly above the S_1 and T_1-T_3 states by about 0.6 to 1 eV, even at their own optimized geometry (Fig. 8). However, in the case of **DIB-PhBr** and **DIB-PhMe**, the CT states are stabilized by approx. 0.2 to 0.3 eV (Figs. S4, S5) in comparison to **DIB-Ph**, which makes them more accessible in the substituted systems. The energetic position of the CT states might also be further stabilized by the interaction with the polymer template and by reduction of the dye as should occur during photocatalysis.[26] Therefore, it can be postulated that the CT states play a role in the photochemistry of these systems, *e.g.* by providing a deactivation channel. Such effect should be more pronounced for **DIB-PhBr** and **DIB-PhMe**, which might then lead to a decreased photocatalytic efficiency.

Steady State and Nanosecond Transient Absorption Spectroscopy

Comparison of the steady state (Fig. 9A) and transient spectroscopic data (Fig. 9B) of the photosensitizer in organic solvent (THF), water and embedded in the polymeric template in aqueous media was yields a basic understanding of the interplay between the BODIPY and PDha-g-PEG. The steady state spectrum in THF is marked by a narrow absorption maximum located at 530 nm and a slight shoulder at 500 nm. In 99% water (1% THF), the absorption feature broadened with its maximum shifted to 580 nm. We conclude the red-shift to be primarily due to the formation of **DIB-Ph** aggregates, as previously reported by Rurack and coworkers.[70] In polymeric nanoaggregates in water, the absorption spectrum of **DIB-Ph** partially resembles the spectra in both organic and aqueous media with local maxima at 500 and 550 nm. Nanosecond transient
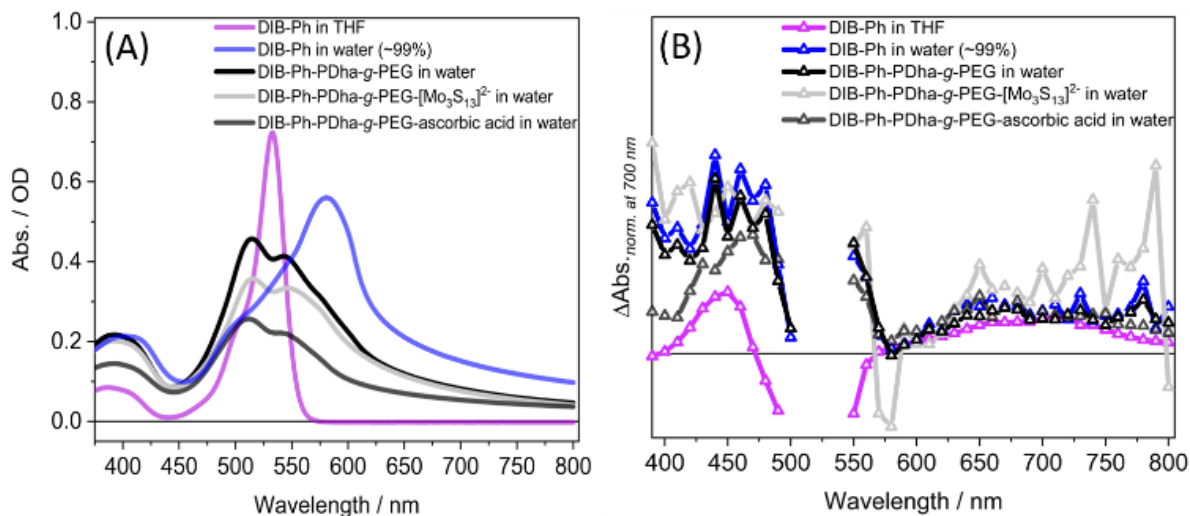

Figure 9. (A) Steady state absorption spectra (B) Nanosecond transient absorption spectra at 2 μs delay time with an excitation wavelength of 530 nm under inert condition of 1. DIB-Ph in THF and water and 2. DIB-Ph incorporated in PDha-g-PEG in water in the absence of ascorbic acid and $[Mo_3S_{13}]^{2-}$, only in the presence of $[Mo_3S_{13}]^{2-}$ and only in the presence of ascorbic acid (concentrations according to the catalytic samples).

absorption spectroscopy yields information regarding states participating in electron transfer reactions during photocatalysis. In principle, electron transfer from a sacrificial electron donor to a PS (reductive quenching) or electron transfer from a PS to a catalyst (oxidative quenching) should lead to a decrease in the lifetime(s) of the excited state(s) compared to the lifetime(s) observed in the absence of such quenching agent(s). Unfortunately, the high scattering from the samples did not allow us to record reliable decay kinetics of the excited state(s) in PDha-*g*-PEG. We instead made use of transient absorption spectra at delay times of 2 µs, to assign spectral features obtained from the transient absorption. The spectra for all samples displayed two prominent excited state absorption (ESA) bands (Fig. 9B), a narrow ESA between 400 and 470 nm and a broad band between 570 and 800 nm. The bands correspond to signatures of BODIPY triplet states[48] which are populated from higher lying singlet states via ISC, a consequence of efficient spin-orbit coupling (SOC) induced by the heavy iodine atom. Additional ESA bands were observed for **DIB-Ph** templated to PDha-*g*-PEG between 550 and 580 nm which is absent for **DIB-Ph** in THF. This differential absorption band is likely due to contributions from **DIB-Ph** aggregates in the polymer. To distinguish the transient absorption features of monomeric **DIB-Ph** from aggregates, nanosecond transient absorption spectra of **DIB-Ph** in 99% water (1% THF) were recorded, an environment in which **DIB-Ph** is prone to aggregation.[70] An identical ESA band between 550 and 580 nm was observed indicating contributions from aggregates to the overall transient absorption spectrum of **DIB-Ph** within the polymer.

21

Conclusions

We developed a photosynthetic platform that operates with cheap, well-known organic chromophores as the light-active component and avoids noble metals in the catalytically active center. Besides PS and CAT, our approach involves a polyampholytic graft copolymer (PDha-*g*-PEG) as unimolecular soft matter matrix, both acting as solubilizing agent for photo-active components and providing close spatial proximity. The reported system displayed high photocatalytic activity in aqueous media, however, the activity was boosted by adding 50% methanol to the catalytic solutions. A series of iodinated BODIPY dyes with different *meso* substituents was employed as organic PSs, including electron donating and withdrawing aryl substituents, heteroaryl substituents, halide-substituted aryl as well as a sole hydrogen to demonstrate the robustness and versatility of the platform. The variety of successfully applied substituents in the photoactive components aims at further modification of the setup towards soft matter and/ or catalyst integration. UV/Vis absorption, fluorescence emission spectroscopy, cyclic voltammetry and quantum chemical simulations displayed minor influence of the *meso* substituent to the optical and electrochemical properties.

In combination with $[Mo_3S_{13}]^{2-}$ as catalyst, **DIB-Ph** showed by far superior activity with a *TON* of 7389 over 16 h, corresponding to an overall *TOF* of 461.8 h^{-1}. With these measures of activity, **DIB-Ph** is well within the range of the highest reported *TON* for organic PSs.[68] What stands out is the *TOF* of the reported system, which is only topped by the benchmark molecular noble metal PS $[Ru(bpy)_3]^{2+}$.[54] **DIB-Ph** was further investigated by TDDFT as well as by steady state and transient absorption spectroscopy in different environments. The investigation indicates that the photocatalytic system in the presented polymeric environment profits from features of both monomeric and aggregated photosensitizer. TDDFT simulations hint that substitution of the

22

phenyl ring in the *meso* position (*e.g.* **DIB-PhBr**) results in an energetically more accessible CT state (in comparison to **DIB-Ph**), which indicates additional excited-state relaxation pathways competing with electron transfer. Substituted **DIB** (*e.g.* **DIB-PhOH**) showed high photocatalytic activity and the substituent can be utilized to modify the described setup.

ASSOCIATED CONTENT

Supporting Information. The following files are available free of charge.

Additional experimental details, materials and methods (word file)

AUTHOR INFORMATION

Corresponding Author

*Daniel Costabel – Friedrich Schiller University Jena, Institute of Organic and Macromolecular Chemistry, Lessingstraße 8, 07743 Jena, Germany, daniel.oliver.costabel@uni-jena.de

*Kalina Peneva – Friedrich Schiller University Jena, Institute of Organic and Macromolecular Chemistry, Lessingstraße 8, 07743 Jena, Germany, kalina.peneva@uni-jena.de

Author Contributions

The manuscript was written through contributions of all authors. All authors have given approval to the final version of the manuscript.

‡D.C. and A.N. contributed equally.

Notes

The authors declare no conflict of interest.

REFERENCES

1. Tachibana, Y.; Vayssieres, L.; Durrant, J. R., Artificial Photosynthesis for Solar Water-splitting. *Nat. Photonics* **2012,** *6*, 511-518.

2. Berardi, S.; Drouet, S.; Francas, L.; Gimbert-Surinach, C.; Guttentag, M.; Richmond, C.; Stoll, T.; Llobet, A., Molecular Artificial Photosynthesis. *Chem. Soc. Rev.* **2014,** *43*, 7501-19.

3. Lang, P.; Habermehl, J.; Troyanov, S. I.; Rau, S.; Schwalbe, M., Photocatalytic Generation of Hydrogen Using Dinuclear pi-Extended Porphyrin-Platinum Compounds. *Chem. Eur. J.* **2018,** *24*, 3225-3233.

4. Martynow, M.; Kupfer, S.; Rau, S.; Guthmuller, J., Excited State Properties of a Series of Molecular PPhotocatalysts investigated by Time Dependent Density Functional Theory. *Phys. Chem. Chem. Phys.* **2019,** *21*, 9052-9060.

5. Bodedla, G. B.; Tritton, D. N.; Chen, X.; Zhao, J.; Guo, Z.; Leung, K. C.-F.; Wong, W.-Y.; Zhu, X., Cocatalyst-free Photocatalytic Hydrogen Evolution with Simple Heteroleptic Iridium(III) Complexes. *ACS. Appl. Energy Mater.* **2021**, *4*, 3945-3951.

6. Zheng, K.; Bodedla, G. B.; Hou, Y.; Zhang, J.; Liang, R.; Zhao, J.; Lee Phillips, D.; Zhu, X., Enhanced Cocatalyst-free Photocatalytic H2 Evolution by the Synergistic AIE and FRET for an Ir-complex Conjugated Porphyrin. *J. Mater. Chem. A* **2022**, *10*, 4440-4445.

7. Bodedla, G. B.; Dong, Y.; Tang, G.; Zhao, J.; Zhang, F.; Zhu, X.; Wong, X.-W., Long-lived Excited States of Platinum(II)-Porphyrins for Highly Efficient Photocatalytic Hydrogen Evolution. *J. Mater. Chem. A* **2022**, *10*, 13402-13409.

8. Chen, Y.; Qu, Y.; Zhou, X.; Li, D.; Xu, P.; Sun, J., Phenyl-Bridged Graphitic Carbon Nitride with a Porous and Hollow Sphere Structure to Enhance Dissociation of Photogenerated Charge Carriers and Visible-Light-Driven H2 Generation. *ACS Appl. Mater. Interfaces* **2020,** *12*, 41527-41537.

9. Li, C.; Hofmeister, E.; Krivtsov, I.; Mitoraj, D.; Adler, C.; Beranek, R.; Dietzek, B., Photodriven Charge Accumulation and Carrier Dynamics in a Water-Soluble Carbon Nitride Photocatalyst. *ChemSusChem* **2021**, *14*, 1728-1736.

10. Abul-Futouh, H.; Zagranyarski, Y.; Muller, C.; Schulz, M.; Kupfer, S.; Gorls, H.; El-Khateeb, M.; Grafe, S.; Dietzek, B.; Peneva, K.; Weigand, W., [FeFe]-Hydrogenase H-cluster Mimics Mediated by Naphthalene Monoimide Derivatives of peri-substituted Dichalcogenides. *Dalton Trans.* **2017,** *46*, 11180-11191.

11. Abul-Futouh, H.; Skabeev, A.; Botteri, D.; Zagranyarski, Y.; Görls, H.; Weigand, W.; Peneva, K., Toward a Tunable Synthetic [FeFe]-Hydrogenase H-Cluster Mimic Mediated by Perylene Monoimide Model Complexes: Insight into Molecular Structures and Electrochemical Characteristics. *Organometallics* **2018,** *37*, 3278-3285.

12. Rauchfuss, T. B., Diiron Azadithiolates as Models for the [FeFe]-Hydrogenase Active Site and Paradigm for the Role of the Second Coordination Sphere. *Acc. Chem. Res.* **2015,** *48*, 2107-16.

13. Ahmed, M. E.; Nayek, A.; Krizan, A.; Coutard, N.; Morozan, A.; Ghosh Dey, S.; Lomoth, R.; Hammarstrom, L.; Artero, V.; Dey, A., A Bidirectional Bioinspired [FeFe]-Hydrogenase Model. *J. Am. Chem. Soc.* **2022,** *144*, 3614-3625.

14. Grutza, M.-L.; Rajagopal, A.; Streb, C.; Kurz, P., Hydrogen Evolution Catalysis by Molybdenum Sulfides (MoSx): are Thiomolybdate Clusters like [Mo3S13]2− Suitable Active Site Models? *Sustainable Energy Fuels* **2018,** *2*, 1893-1904.

15. Rajagopal, A.; Akbarzadeh, E.; Li, C.; Mitoraj, D.; Krivtsov, I.; Adler, C.; Diemant, T.; Biskupek, J.; Kaiser, U.; Im, C.; Heiland, M.; Jacob, T.; Streb, C.; Dietzek, B.; Beranek, R., Polymeric Carbon Nitride Coupled with a Molecular Thiomolybdate Catalyst: Exciton and Charge Dynamics in Light-driven Hydrogen Evolution. *Sustainable Energy Fuels* **2020,** *4*, 6085-6095.

16. Bold, S.; Straistari, T.; Muñoz-García, A. B.; Pavone, M.; Artero, V.; Chavarot-Kerlidou, M.; Dietzek, B., Investigating Light-Induced Processes in Covalent Dye-Catalyst Assemblies for Hydrogen Production. *Catalysts* **2020,** *10*, 1340.

17. Gueret, R.; Poulard, L.; Oshinowo, M.; Chauvin, J.; Dahmane, M.; Dupeyre, G.; Lainé, P. P.; Fortage, J.; Collomb, M.-N., Challenging the [Ru(bpy)3]2+ Photosensitizer with a Triazatriangulenium Robust Organic Dye for Visible-Light-Driven Hydrogen Production in Water. *ACS Catal.* **2018,** *8*, 3792-3802.

18. Larsen, C. B.; Wenger, O. S., Photoredox Catalysis with Metal Complexes Made from Earth-Abundant Elements. *Chem. Eur. J* **2018,** *24*, 2039-2058.

19. Wenger, O. S., Photoactive Complexes with Earth-Abundant Metals. *J. Am. Chem. Soc.* **2018,** *140*, 13522-13533.

20. Weingarten, A. S.; Kazantsev, R. V.; Palmer, L. C.; McClendon, M.; Koltonow, A. R.; Samuel, A. P.; Kiebala, D. J.; Wasielewski, M. R.; Stupp, S. I., Self-assembling Hydrogel Scaffolds for Photocatalytic Hydrogen Production. *Nat. Chem.* **2014,** *6*, 964-70.

21. Max, J. B.; Kowalczuk, K.; Köhler, M.; Neumann, C.; Pielenz, F.; Sigolaeva, L. V.; Pergushov, D. V.; Turchanin, A.; Langenhorst, F.; Schacher, F. H., Polyampholytic Poly(dehydroalanine) Graft Copolymers as Smart Templates for pH-Controlled Formation of Alloy Nanoparticles. *Macromolecules* **2020,** *53*, 4511-4523.

22. Costabel, D.; Skabeev, A.; Nabiyan, A.; Luo, Y.; Max, J. B.; Rajagopal, A.; Kowalczyk, D.; Dietzek, B.; Wachtler, M.; Gorls, H.; Ziegenbalg, D.; Zagranyarski, Y.; Streb, C.; Schacher, F. H.; Peneva, K., 1,7,9,10-Tetrasubstituted PMIs Accessible through Decarboxylative Bromination: Synthesis, Characterization, Photophysical Studies, and Hydrogen Evolution Catalysis. *Chem. Eur. J.* **2021,** *27*, 4081-4088.

23. Nabiyan, A.; Max, J. B.; Neumann, C.; Heiland, M.; Turchanin, A.; Streb, C.; Schacher, F. H., Polyampholytic Graft Copolymers as Matrix for TiO2 /Eosin Y/[Mo3 S13](2-) Hybrid Materials and Light-Driven Catalysis. *Chem. Eur. J.* **2021**, *27*, 16924-16929.

24. Loudet, A.; Burgess, K., BODIPY Dyes and Their Derivatives: Synthesis and Spectroscopic Properties. *Chem. Rev.* **2007,** *107*, 4891-4932.

25. Zhao, J.; Xu, K.; Yang, W.; Wang, Z.; Zhong, F., The Triplet Excited State of Bodipy: Formation, Modulation and Application. *Chem. Soc. Rev.* **2015,** *44*, 8904-39.

26. K. Ziems; S. Gräfe; S. Kupfer, Photo-Induced Charge Separation vs. Degradation of a BODIPY-Based Photosensitizer Assessed by TDDFT and RASPT2. *Catalysts* **2018,** *8*, 520.

27. Beaudet, A.; Nouel, D.; Stroh, T.; Vandenbulcke, F.; Dal-Farra, C.; Vincent, J.-P., Fluorescent Ligands for Studying Neuropeptide Receptors by Confocal Microscopy. *Braz. J. Med. Biol. Res.* **1998,** *31*, 1479-1489.

28. Pagano, R. E.; Chen, C.-S., Use of BODIPY-labeled Sphingolipids to Study Membrane Traffic along the Endocytic Pathway. *Ann. N. Y. Acad. Sci.* **1998,** *845*, 152-160.

29. Kowada, T.; Maeda, H.; Kikuchi, K., BODIPY-based Probes for the Fluorescence Imaging of Biomolecules in Living Cells. *Chem. Soc. Rev.* **2015,** *44*, 4953-72.

30. Kamkaew, A.; Lim, S. H.; Lee, H. B.; Kiew, L. V.; Chung, L. Y.; Burgess, K., BODIPY Dyes in Photodynamic Therapy. *Chem. Soc. Rev.* **2013,** *42,* 77-88.

31. Awuah, S. G.; You, Y., Boron Dipyrromethene (BODIPY)-based Photosensitizers for Photodynamic Therapy. *RSC Adv.* **2012,** *2*, 11169-11183.

32. Wu, W.; Sun, J.; Cui, X.; Zhao, J., Observation of the Room Temperature Phosphorescence of Bodipy in Visible Light-harvesting Ru(II) Polyimine Complexes and Application as Triplet Photosensitizers for Triplet–Triplet-Annihilation Upconversion and Photocatalytic Oxidation. *J. Mater. Chem. C* **2013,** *1*, 4577-4589.

33. Wu, W.; Guo, H.; Wu, W.; Ji, S.; Zhao, J., Organic Triplet Sensitizer Library derived from a single Chromophore (BODIPY) with Long-lived Triplet Excited State for Triplet-Triplet Annihilation based Upconversion. *J. Org. Chem.* **2011,** *76*, 7056-64.

34. Squeo, B. M.; Ganzer, L.; Virgili, T.; Pasini, M., BODIPY-Based Molecules, a Platform for Photonic and Solar Cells. *Molecules* **2020,** *26,* 153.

35. Roncali, J., Molecular Bulk Heterojunctions: An Emerging Approach to Organic Solar Cells. *Acc. Chem. Res.* **2099,** *42*, 1719-1730.

36. Erten-Ela, S.; Deniz Yilmaz, M.; Icli, B.; Dede, Y.; Icli, S.; Akkaya, E. U., A Panchromatic Boradiazaindacene (BODIPY) Sensitizer for Dye-Sensitized Solar Cells. *Org. Lett.* **2008,** *10*, 3299-3302.

37. Ooyama, Y.; Hagiwara, Y.; Mizumo, T.; Harima, Y.; Ohshita, J., Photovoltaic Performance of Dye-Sensitized Solar Cells based on D–π–A Type BODIPY Dye with two Pyridyl Groups. *New J. Chem.* **2013,** *37*, 2479-2485.

38. De Bonfils, P.; Péault, L.; Nun, P.; Coeffard, V., State of the Art of Bodipy-Based Photocatalysts in Organic Synthesis. *Eur. J. Org. Chem.* **2021,** *2021*, 1809-1824.

39. Li, H.; Zhou, M.; Chen, Q.-Y.; Liu, X.-Y.; Kan, X.-L.; Sun, M.; Qu, L.-L., BODIPY Functional Metal–Organic-Frameworks for Efficient Visible-light-driven Water Oxidation without Additional Photosensitizers. *Sustainable Energy Fuels* **2021,** *5*, 1779-1785.

40. Huang, L.; Zhao, J.; Guo, S.; Zhang, C.; Ma, J., Bodipy Derivatives as Organic Triplet Photosensitizers for Aerobic Photoorganocatalytic Oxidative Coupling of Amines and Photooxidation of Dihydroxylnaphthalenes. *J. Org. Chem.* **2013,** *78*, 5627-37.

41. Xie, A.; Pan, Z.-H.; Yu, M.; Luo, G.-G.; Sun, D., Photocatalytic Hydrogen Production from Acidic Aqueous Solution in BODIPY-Cobaloxime-Ascorbic Acid Homogeneous System. *Chin. Chem. Lett.* **2019,** *30*, 225-228.

42. Cullen, A. A.; Heintz, K.; O'Reilly, L.; Long, C.; Heise, A.; Murphy, R.; Karlsson, J.; Gibson, E.; Greetham, G. M.; Towrie, M.; Pryce, M. T., A Time-Resolved Spectroscopic Investigation of a Novel BODIPY Copolymer and Its Potential Use as a Photosensitiser for Hydrogen Evolution. *Front. Chem.* **2020,** *8*, 584060.

43. Bartelmess, J.; Francis, A. J.; El Roz, K. A.; Castellano, F. N.; Weare, W. W.; Sommer, R. D., Light-driven Hydrogen Evolution by BODIPY-Sensitized Cobaloxime Catalysts. *Inorg. Chem.* **2014,** *53*, 4527-34.

44. Luo, G. G.; Fang, K.; Wu, J. H.; Dai, J. C.; Zhao, Q. H., Noble-Metal-Free BODIPY-Cobaloxime Photocatalysts for Visible-Light-Driven Hydrogen Production. *Phys. Chem. Chem. Phys.* **2014,** *16*, 23884-94.

45. Eckenhoff, W. T.; McNamara, W. R.; Du, P.; Eisenberg, R., Cobalt Complexes as Artificial Hydrogenases for the Reductive Side of Water Splitting. *Biochim. Biophys. Acta* **2013,** *1827*, 958-73.

46. Suryani, O.; Higashino, Y.; Sato, H.; Kubo, Y., Visible-to-Near-Infrared Light-Driven Photocatalytic Hydrogen Production Using Dibenzo-BODIPY and Phenothiazine Conjugate as Organic Photosensitizer. *ACS Appl. Energy Mater.* **2018,** *2*, 448-458.

47. Dura, L.; Ahrens, J.; Pohl, M. M.; Hofler, S.; Broring, M.; Beweries, T., Design of BODIPY Dyes as Photosensitisers in Multicomponent Catalyst Systems for Light-Driven Hydrogen Production. *Chem. Eur. J.* **2015,** *21*, 13549-52.

48. Dura, L.; Wächtler, M.; Kupfer, S.; Kübel, J.; Ahrens, J.; Höfler, S.; Bröring, M.; Dietzek, B.; Beweries, T., Photophysics of BODIPY Dyes as Readily-Designable Photosensitisers in Light-Driven Proton Reduction. *Inorganics* **2017,** *5*, 21.

49. Larzarides, T.; McCormick, T. M.; Wilson, K. C.; Lee, S.; McCamant, D. M.; Eisenberg, R., Sensitizing the Sensitizer: The Synthesis and Photophysical Study of Bodipy-Pt(II)diimine(dithiolate) Conjugates. *J. Am. Chem. Soc.* **2011,** *133*, 350-364.

50. Zheng, B.; Sabatini, R. P.; Fu, W. F.; Eum, M. S.; Brennessel, W. W.; Wang, L.; McCamant, D. W.; Eisenberg, R., Light-Driven Generation of Hydrogen: New Chromophore Dyads for Increased Activity based on Bodipy Dye and Pt(diimine)(dithiolate) Complexes. *Proc. Natl. Acad. Sci. U.S.A.* **2015,** *112*, E3987-96.

51. Black, F. A.; Jacquart, A.; Toupalas, G.; Alves, S.; Proust, A.; Clark, I. P.; Gibson, E. A.; Izzet, G., Rapid Photoinduced Charge Injection into Covalent Polyoxometalate-Bodipy Conjugates. *Chem. Sci.* **2018,** *9*, 5578-5584.

52. Cetindere, S.; Clausing, S. T.; Anjass, M.; Luo, Y.; Kupfer, S.; Dietzek, B.; Streb, C., Covalent Linkage of BODIPY-Photosensitizers to Anderson-Type Polyoxometalates Using CLICK Chemistry. *Chem. Eur. J.* **2021**, *27*, 17181-17187.

53. Rajagopal, A.; Venter, F.; Jacob, T.; Petermann, L.; Rau, S.; Tschierlei, S.; Streb, C., Homogeneous Visible Light-Driven Hydrogen Evolution by the Molecular Molybdenum Sulfide Model [Mo2S12]2−. *Sustainable Energy Fuels* **2019,** *3*, 92-95.

54. Dave, M.; Rajagopal, A.; Damm-Ruttensperger, M.; Schwarz, B.; Nägele, F.; Daccache, L.; Fantauzzi, D.; Jacob, T.; Streb, C., Understanding Homogeneous Hydrogen Evolution Reactivity and Deactivation Pathways of Molecular Molybdenum Sulfide Catalysts. *Sustainable Energy Fuels* **2018,** *2*, 1020-1026.

55. Karges, J.; Basu, U.; Blacque, O.; Chao, H.; Gasser, G., Polymeric Encapsulation of Novel Homoleptic Bis(dipyrrinato) Zinc(II) Complexes with Long Lifetimes for Applications as Photodynamic Therapy Photosensitisers. *Angew. Chem. Int. Ed. Engl.* **2019,** *58*, 14334-14340.

56. Aydin Tekdas, D.; Viswanathan, G.; Zehra Topal, S.; Looi, C. Y.; Wong, W. F.; Min Yi Tan, G.; Zorlu, Y.; Gurek, A. G.; Lee, H. B.; Dumoulin, F., Antimicrobial Activity of a Quaternized BODIPY against Staphylococcus Strains. *Org. Biomol. Chem.* **2016,** *14*, 2665-70.

57. Wang, M.; Zhang, Y.; Wang, T.; Wang, C.; Xue, D.; Xiao, J., Story of an Age-Old Reagent: An Electrophilic Chlorination of Arenes and Heterocycles by 1-Chloro-1,2-benziodoxol-3-one. *Org. Lett.* **2016,** *18*, 1976-9.

58. Shao, S.; Thomas, M. B.; Park, K. H.; Mahaffey, Z.; Kim, D.; D'Souza, F., Sequential Energy Transfer Followed by Electron Transfer in a BODIPY-BisstyrylBODIPY bound to C60 Triad via a 'Two-Point' Binding Strategy. *Chem. Commun. (Camb.)* **2017,** *54*, 54-57.

59. Hu, W.; Ma, H.; Hou, B.; Zhao, H.; Ji, Y.; Jiang, R.; Hu, X.; Lu, X.; Zhang, L.; Tang, Y.; Fan, Q.; Huang, W., Engineering Lysosome-Targeting BODIPY Nanoparticles for Photoacoustic Imaging and Photodynamic Therapy under Near-Infrared Light. *ACS Appl. Mater. Interfaces* **2016,** *8*, 12039-47.

60. Ustinov, A.; Korshun, V.; Samoilichenko, Y.; Larkin, D.; Mariewskaya, K. A., Fluorescence of BODIPY Dyes in Gas Phase at near Ambient Conditions. *ChemRxiv* **2020**, 1-4.

61. Maeda, H.; Nishimura, Y.; Hiroto, S.; Shinokubo, H., Assembled Structures of Dipyrrins and their Oligomers Bridged by Dioxy-Boron Moieties. *Dalton Trans.* **2013,** *42*, 15885-8.

62. Gibbs, J. H.; Robins, L. T.; Zhou, Z.; Bobadova-Parvanova, P.; Cottam, M.; McCandless, G. T.; Fronczek, F. R.; Vicente, M. G., Spectroscopic, Computational Modeling and Cytotoxicity of a Series of Meso-Phenyl and Meso-Thienyl-BODIPYs. *Bioorg. Med. Chem.* **2013,** *21*, 5770-81.

63. Sittig, M.; Schmidt, B.; Gorls, H.; Bocklitz, T.; Wachtler, M.; Zechel, S.; Hager, M. D.; Dietzek, B., Fluorescence Upconversion by Triplet-Triplet Annihilation in All-Organic Poly(methacrylate)-Terpolymers. *Phys. Chem. Chem. Phys.* **2020,** *22*, 4072-4079.

64. Özcan, E.; Dedeoglu, B.; Chumakov, Y.; Gürek, A. G.; Zorlu, Y.; Çoşut, B.; Menaf Ayhan, M., Halogen-Bonded BODIPY Frameworks with Tunable Optical Features**. *Chem. Eur. J.* **2020,** *27*, 1603-1608.

65. Pellegrin, Y.; Odobel, F., Sacrificial Electron Donor Reagents for Solar Fuel Production. *C. R. Chim.* **2017,** *20*, 283-295.

66. Lei, Y.; Yang, M.; Hou, J.; Wang, F.; Cui, E.; Kong, C.; Min, S., Thiomolybdate [Mo3S13](2-) Nanocluster: a Molecular Mimic of MoS2 Active Sites for Highly Efficient Photocatalytic Hydrogen Evolution. *Chem. Commun.* **2018,** *54*, 603-606.

67. Weingarten, A. S.; Dannenhoffer, A. J.; Kazantsev, R. V.; Sai, H.; Huang, D.; Stupp, S. I., Chromophore Dipole Directs Morphology and Photocatalytic Hydrogen Generation. *J. Am. Chem. Soc.* **2018,** *140*, 4965-4968.

68. Kazantsev, R. V.; Dannenhoffer, A. J.; Weingarten, A. S.; Phelan, B. T.; Harutyunyan, B.; Aytun, T.; Narayanan, A.; Fairfield, D. J.; Boekhoven, J.; Sai, H.; Senesi, A.; O'Dogherty, P. I.; Palmer, L. C.; Bedzyk, M. J.; Wasielewski, M. R.; Stupp, S. I., Crystal-Phase Transitions and Photocatalysis in Supramolecular Scaffolds. *J. Am. Chem. Soc.* **2017,** *139*, 6120-6127.

69. Heiland, M.; De, R.; Rau, S.; Dietzek-Ivansic, B.; Streb, C., Not that Innocent - Ammonium Ions Boost Homogeneous Light-Driven Hydrogen Evolution. *Chem. Commun. (Camb.)* **2022,** *58*, 4603-4606.

70. Descalzo, A. B.; Ashokkumar, P.; Shen, Z.; Rurack, K., On the Aggregation Behaviour and Spectroscopic Properties of Alkylated and Annelated Boron-Dipyrromethene (BODIPY) Dyes in Aqueous Solution. *ChemPhotoChem* **2019,** *4*, 120-131.